A&A 532, A130 (2011)
DOI: 10.1051/0004-6361/201117069

Astronomy & Astrophysics

The spectrum of (136199) Eris between 350 and 2350 nm: results with X-Shooter⋆

A. Alvarez-Candal[1], N. Pinilla-Alonso[2], J. Licandro[3,4], J. Cook[2], E. Mason[5], T. Roush[6], D. Cruikshank[6], F. Gourgeot[1], E. Dotto[7], and D. Perna[8]

[1] European Southern Observatory, Alonso de Córdova 3107, Vitacura, Casilla 19001, Santiago 19, Chile
e-mail: aalvarez@eso.org
[2] NASA Post-Doctoral Program, Resident Research Associated at NASA Ames Research Center, Moffett Field, CA, USA
[3] Instituto de Astrofísica de Canarias, c/vía Láctea s/n, 38200 La Laguna, Tenerife, Spain
[4] Departamento de Astrofísica, Universidad de La Laguna, 38205 La Laguna, Tenerife, Spain
[5] Space Telescope Science Institute, 3700 San Martin Dr., Baltimore MD 21218, USA
[6] NASA Ames Research Center, Moffett Field, CA, USA
[7] Istituto Nazionale di Astrofisica (INAF), Osservatorio Astronomico di Roma, Italy
[8] Istituto Nazionale di Astrofisica (INAF), Osservatorio Astronomico di Capodimonte, Italy

Received 12 April 2011 / Accepted 6 July 2011

ABSTRACT

Context. X-Shooter is the first second-generation instrument for the ESO-Very Large Telescope. It is a spectrograph covering the entire 300−2480 nm spectral range at once with a high resolving power. These properties enticed us to observe the well-known trans-Neptunian object (136199) Eris during the science verification of the instrument. The target has numerous absorption features in the optical and near-infrared domain that have been observed by different authors, showing differences in these features' positions and strengths.
Aims. Besides testing the capabilities of X-Shooter to observe minor bodies, we attempt to constrain the existence of super-volatiles, e.g., CH_4, CO and N_2, and in particular we try to understand the physical-chemical state of the ices on Eris' surface.
Methods. We observed Eris in the 300−2480 nm range and compared the newly obtained spectra with those available in the literature. We identified several absorption features, measured their positions and depth, and compare them with those of the reflectance of pure methane ice obtained from the optical constants of this ice at 30 K to study shifts in these features' positions and find a possible explanation for their origin.
Results. We identify several absorption bands in the spectrum that are all consistent with the presence of CH_4 ice. We do not identify bands related to N_2 or CO. We measured the central wavelengths of the bands and compared to those measured in the spectrum of pure CH_4 at 30 K finding variable spectral shifts.
Conclusions. Based on these wavelength shifts, we confirm the presence of a dilution of CH_4 in other ice on the surface of Eris and the presence of pure CH_4 that is spatially segregated. The comparison of the centers and shapes of these bands with previous works suggests that the surface is heterogeneous. The absence of the 2160 nm band of N_2 can be explained if the surface temperature is below 35.6 K, the transition temperature between the alpha and beta phases of this ice. Our results, including the reanalysis of data published elsewhere, point to a heterogeneous surface on Eris.

Key words. Kuiper belt objects: individual: (136199) Eris – instrumentation: spectrographs – techniques: spectroscopic

1. Introduction

To interpret the surface composition of minor bodies, it is necessary to observe their spectra in the widest possible spectral range. This is typically achieved by observing the target with different instruments, techniques, and calibrations. This results in a lack of simultaneous datasets and in having often to rely on other parameters (e.g., albedo, photometric magnitudes) to scale the complete spectrum. Luckily, new instrumentation allows us to overcome some of these problems. One of these new instruments is X-Shooter (XS), which is also the first second-generation instrument developed for the ESO-Very Large Telescope (D'Odorico et al. 2006) and is currently mounted in its unit 2 (Kueyen).

A more detailed discussion of XS is given in Sect. 2, but, briefly, XS is a spectrograph that obtains spectra from 300 to 2480 nm in a single shot at high resolving powers (from 3000 up to 10 000). This wavelength range sufficiently covers many known ices and silicates. At the time of its science verification we decided to test its capabilities by observing a well-known trans-Neptunian object with absorption features in most of this spectral range: (136199) Eris (hereafter Eris).

Eris, formerly known as 2003 UB_{313}, is one of the largest bodies in the trans-Neptunian region, with a diameter <2340 km (B. Sicardy, priv. comm.), and, together with two of the other thousand-km-sized objects [(134340) Pluto and (136472) Makemake], shows CH_4 absorption bands in the spectrum from the visible to the near infrared (see Brown et al. 2005; Licandro et al. 2006).

Rotational light-curves of Eris have had little success in obtaining a reliable rotational period (e.g., Carraro et al. 2006; or Duffard et al. 2008). Roe et al. (2008) proposed a rotational period of 1.08 days. The light-curve seems to be unrelated to Eris' shape, but probably belongs to an albedo patch. Nevertheless,

⋆ Observations made during X-Shooter Science Verification, program 60.A-9400(A), PIs: Alvarez-Candal and Mason.

Table 1. Observational circumstances.

Date[a]	Airmass[b]	Seeing[b] ($''$)	t_{UVB} (s)	t_{VIS} (s)	t_{NIR} (s)	Star (Airmass)
2009-08-14UT07:24	1.073–1.146	0.7–0.8	2×1680	2×1680	2×1800	SA93-101 (1.113)
2009-09-29UT05:50	1.065–1.163	0.9–1.2	2×1680	2×1680	2×1800	SA93-101 (1.153)

Notes. We show the exposure time per each arm, t_{ARM}. [(a)] Beginning of the observation. [(b)] Minimum and maximum values during the span of the observation.

owing to the noise in the data, even if this albedo patch indeed exists, clearly, there are no significant albedo heterogeneities.

A close look at the spectroscopic data shows that there is a subtle heterogeneity, however. Abernathy et al. (2009) compared their spectra with those of Licandro et al. (2006), finding different central wavelengths and different depths for a few selected methane absorption bands. Nevertheless, recent results point in another direction: Tegler et al. (2010), using their own results and those of Quirico & Schmitt (1997a), showed that a single component, CH_4 diluted in N_2, could explain the wavelength shifts because those shifts increase with increasing wavelength.

The orbit of Eris is that of a scattered disk-object (Gladman et al. 2008). It has a perihelion distance of 49.5 AU and is currently located at 97 AU and approaching perihelion. At 97 AU, its equilibrium temperature is $\lesssim$30 K as estimated by the Stefan-Boltzman law and assuming conservation of energy. Therefore, based on models of volatile retention (see Schaller & Brown 2007) and its similarities with Pluto, Eris' surface is expected to be covered in N_2, CO, and CH_4 ices. Of these species, only CH_4 has been clearly seen on Eris.

Therefore we requested observing time during the XS science verification to make the most of its high resolving power to detect features of CO and N_2, and to obtain the Eris spectrum simultaneously between 300 and 2480 nm.

The article is organized as follows: in Sect. 2 we describe the instrument and the observations. In Sect. 3 we present the results obtained from our analysis, while the discussion and conclusions are presented in Sects. 4 and 5, respectively.

2. Observation and data reduction

2.1. X-Shooter

The instrument is an *Echelle* spectrograph that has an almost fixed spectral setup. The observer can choose between SLIT (and slit width) and IFU (integral field unit) modes. We used the SLIT mode. The detailed description of the instrument is available at ESO's webpage[1]. This spectrograph has the ability to simultaneously obtain data over the entire 300−2480 nm spectral range by splitting the incoming light from the telescope into three beams, each sent to a different arm: ultra-violet–blue (UVB), visible (VIS), and near-infrared (NIR). Using two dicroichs, the light is first sent to the UVB arm, then the VIS arm, and the remaining light arrives at the NIR arm. The disadvantage of this optical path is the high thermal background in the K-region of the NIR spectrum.

Each arm operates independently of the others, with the sole exception of the two CCDs (UVB and VIS), which are controlled by the same FIERA (Fast Imaging Electronic Readout Assembly). Therefore, if the two exposures finish at the same time, their read-out is made sequentially. The read-out of the NIR detector is totally independent of the others, operated by an IRACE (Infra Red Array Control Electronics) controller.

[1] http://www.eso.org/sci/facilities/paranal/instruments/xshooter/

2.2. The observational setup

We observed Eris on two nights of the XS Science Verification, August 14 and September 29, 2009. As mentioned above, we used the SLIT mode, selecting the high-gain readout mode and 2×1 binning for the UVB and VIS detectors. The read-out and binning for the NIR detector are fixed. The slit widths were $1.0''$, $0.9''$, and $0.9''$, for the UVB, VIS, and NIR arms, respectively, yielding a resolving power of about 5000 per arm. As usual with NIR observations, we nodded on the slit to remove the sky contribution. Because the nod is made by the telescope, we finished with two exposures per arm per night.

To remove the solar and telluric signals from Eris spectra, we observed the G5 star SA93-101 (Landolt 1992) with the same observational setup as Eris and a similar airmass to minimize effects of differential refraction. Details of the observations are presented in Table 1.

2.3. Data reduction

The data presented here were reduced using the XS pipeline (0.9.4). There are newer versions of the pipeline, but we verified after processing the spectra that no significant improvements are obtained in terms of SNR, therefore we used version 0.9.4. The pipeline accounts for flat-fielding, wavelength calibration, merging of different orders, and the extraction of the spectra. The whole reduction relies on calibration files taken during daytime and on a set of static files provided as part of the pipeline release.

The data were wavelength and spatially calibrated by creating a two-dimensional wave-map. This is necessary because of the curvature of the *Echelle* orders. The map was created by taking images of ThAr lamps combined with pinhole masks for all three arms. The final accuracy of the calibration is better than 1 Å throughout the complete spectral range.

After careful evaluation we decided not to use the one-dimensional spectra produced by the pipeline, but instead make our own extraction using a merged two-dimensional spectrum generated during the process. The extraction was made in the usual way with `apall.iraf`.

Once all spectra were extracted, we divided those of Eris by the corresponding star, used as telluric and solar analog star (Table 1). After the division we removed the remaining bad pixels from the spectra using a median filtering technique (as in Alvarez-Candal et al. 2007). This last step left us with three separated spectra, one per arm. Because their spectral ranges overlap slightly, the construction of the final spectrum is straightforward. The resulting spectra between 350 and 2350 nm, normalized to unity at 600 nm, are presented in Fig. 1.

A few of the *Echelle* orders were not well merged, in particular in the visible. We checked that none of them removed

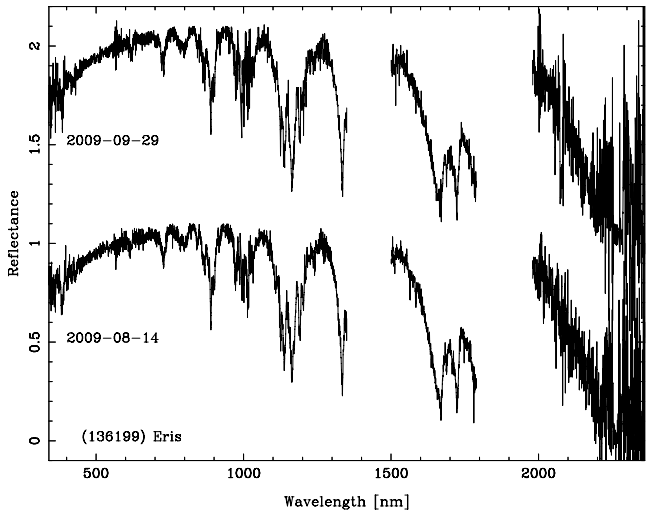

Fig. 1. Eris spectra obtained with X-Shooter. The resolving power is about 5000 for the spectral range. The spectra were arbitrarily normalized to unity at 600 nm. The spectrum of September 2009 was shifted by 1 in the flux scale for clarity. Note that we removed parts with strong atmospheric absorption.

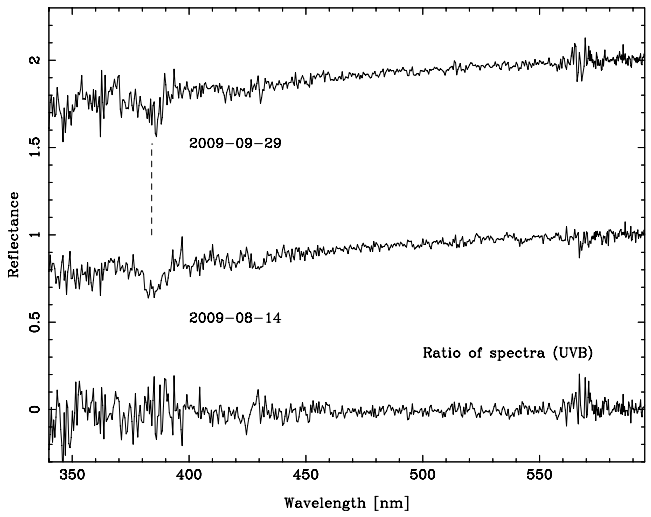

Fig. 2. Ratio of the X-Shooter spectra obtained in the ultra-violet–blue region. The artifacts mentioned in the text are marked with a vertical dashed line. Normalization and offsets are the same as in Fig. 1. At the bottom we show the ratio of both spectra, offset by −1 in the scale for clarity.

important information, e.g., being the minimum or the edge of an absorption band, and decided to ignore them. Two other features at 1576 and 1583 nm, each in a different spectrum, are artifacts introduced by the star and poor telluric correction, respectively. Another feature, at 2160 nm, is due to an order badly merged during the reduction process. Finally, the feature at about 400 nm is introduced by the star (Alvarez-Candal et al. 2008) and does not represent any compound present on Eris surface. All these features are marked in Figs. 2 to 4.

3. Spectroscopic analysis

The spectra presented in Fig. 1 are similar throughout the complete wavelength range, as shown by the low residues resulting from the calculated ratio of both spectra (Figs. 2–4). They both

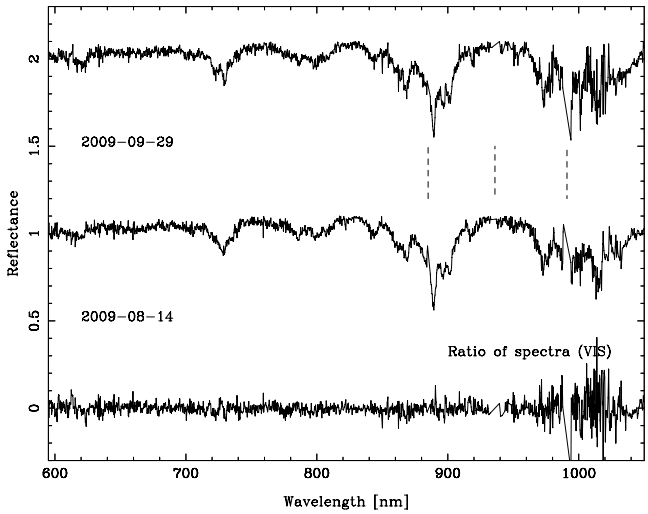

Fig. 3. Same as Fig. 2 but showing only the visible region.

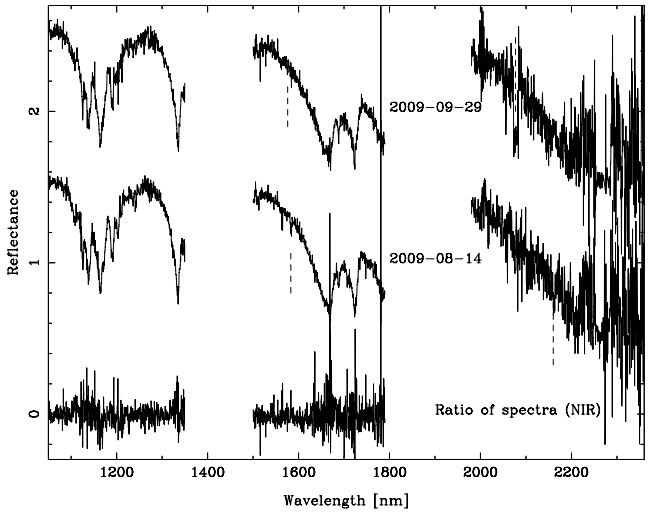

Fig. 4. Same as Fig. 2 but showing the near-infrared region. The normalization is the same as in Fig. 1, but we applied offsets of 0.5 and 1.5 in the flux scale for the August and September 2009 spectra, respectively, for clarity. The ratio of the spectra is not shown in the K-region owing to low SNR.

present clear CH_4 absorptions from the visible up to the near-infrared and have similar spectral slopes in the visible (see first row of Table 2).

One interesting absorption detected in the Eris spectra is located at 620 nm. This band has been observed in all the giant planets and in Titan's spectrum and it appears in other previously published spectra of Eris, but has not been discussed. The band has been assigned to CH_4 in its gaseous (Giver 1978) and liquid (Ramaprasad et al. 1978; Patel et al. 1980) phases in laboratory experiments. The band strength is ∼1 order of magnitude smaller than the 730 nm band, thus, its appearance certainly suggests relatively long path-lengths, and likely high concentrations of CH_4.

At first glance, these data also resemble those already available in the literature, for example: Licandro et al. (2006), Alvarez-Candal et al. (2008) in the visible; Dumas et al. (2007), Guilbert et al. (2009), and Merlin et al. (2009) in the near-infrared. These similarities indicate that there are no spectral differences within the uncertainties of the data, suggesting an

Table 2. Comparison of spectral parameters: spectral slope in the visible, S'_v, in % (100 nm)$^{-1}$, and percentile depth of the absorption feature, D_λ at a given wavelength λ.

Band (nm)	*a* (%)	*b* (%)	*c* (%)	*d* (%)	*e* (%)	*f* (%)	*g* (%)	*h* (%)
S'_v	3.8 ± 1.1	(...)	3.4 ± 0.5	2.9 ± 0.6	(...)	(...)	(...)	12.5 ± 1.2
620	5.3 ± 1.0	(...)	3.9 ± 3.7	4.7 ± 1.0	(...)	(...)	(...)	Undet.
730	15.8 ± 1.8	15.0 ± 4.6	15.7 ± 5.2	15.1 ± 2.0	(...)	(...)	(...)	5.6 ± 1.1
790	9.7 ± 0.7	8.1 ± 3.6	8.8 ± 3.3	7.2 ± 0.8	(...)	(...)	(...)	Undet.
840	5.9 ± 1.4	Undet.	8.2 ± 5.4	5.4 ± 1.1	(...)	(...)	(...)	2.7 ± 0.9
870	13.2 ± 1.8	15.1 ± 1.4	19.0 ± 7.5	14.1 ± 1.1	(...)	(...)	(...)	3.8 ± 3.3
890	46.3 ± 1.4	35.1 ± 7.6	55.9 ± 8.8	41.8 ± 3.9	(...)	(...)	(...)	16.2 ± 1.1
1000	20.2 ± 8.3	(...)	(...)	(...)	(...)	(...)	(...)	(...)
1015	31.2 ± 4.3	(...)	(...)	(...)	(...)	(...)	(...)	(...)
1135	39.3 ± 2.1	(...)	(...)	(...)	(...)	(...)	(...)	(...)
1160	54.5 ± 5.0	(...)	(...)	(...)	(...)	(...)	(...)	(...)
1190	34.4 ± 2.0	(...)	(...)	(...)	(...)	(...)	(...)	(...)
1240	9.0 ± 0.9	(...)	(...)	(...)	(...)	(...)	(...)	(...)
1335	72.2 ± 2.6	(...)	(...)	(...)	(...)	(...)	(...)	(...)
1485	(...)	(...)	(...)	(...)	18.9 ± 5.8	32.1 ± 1.7	31.1 ± 0.9	12.9 ± 0.9
1670	64.4 ± 7.3	(...)	(...)	(...)	61.2 ± 9.5	77.7 ± 7.5	82.1 ± 8.3	59.1 ± 2.9
1690	17.4 ± 4.8	(...)	(...)	(...)	15.5 ± 6.1	16.3 ± 6.8	14.6 ± 2.2	5.3 ± 0.2
1720	66.2 ± 7.3	(...)	(...)	(...)	53.6 ± 10.9	68.3 ± 5.4	59.2 ± 3.0	50.2 ± 1.2
1800	Undet.	(...)	(...)	(...)	66.8 ± 4.8	72.4 ± 13.7	70.3 ± 3.4	56.0 ± 0.6
2200	Undet.	(...)	(...)	(...)	89.5 ± 29.2	81.1 ± 18.1	60.4 ± 8.4	50.7 ± 1.1

Notes. Undet. = undetermined; references: (*a*) this work; (*b*) Abernathy et al. (2009); (*c*) Licandro et al. (2006); (*d*) Alvarez-Candal et al. (2008); (*e*) Guilbert et al. (2009); (*f*) Merlin et al. (2009); (*g*) Dumas et al. (2007); (*h*) Merlin et al. (2010), Pluto.

a priori homogeneous surface. With this in mind, and along with the datasets mentioned above, we will use a combined spectrum of Eris, obtained as the average of the two XS spectra, unless explicitly mentioned otherwise.

3.1. Quantitative interpretation of the spectra

In order to quantify the information in the Eris spectrum, we determined a number of spectral parameters, which are listed in Table 2.

All measurements presented below were made by our team. We preferred, for the sake of keeping the data as homogeneous as possible, to measure all quantities rather than use published values. Along with our Eris data we present values obtained for other Eris spectra, see below, and Pluto (column labeled *h*), these last data are taken from Merlin et al. (2010, their April 13, 2008 spectrum).

The Eris spectra we used are: *visible* from Licandro et al. (2006), Alvarez-Candal et al. (2008, their October 2006 spectrum), and Abernathy et al. (2009, both spectra); and *near-infrared* from Dumas et al. (2007), Guilbert et al. (2009), and Merlin et al. (2009, their December 2007 spectrum).

We use the shorthand term "organics" to denote the relatively refractory solid material consisting of complex macromolecular carbonaceous material that is similar to the insoluble organic matter found in most carbonaceous meteorites. This material contains both aromatic and aliphatic hydrocarbons, amorphous carbon, and other materials of undetermined structure. Organics of this general kind characteristically have very low albedo (~0.02−0.06) and distinctive red color in the spectral region 300−1000 nm.

We measured the spectral slope, which provides an indication of the presence of organic materials. To compute it we fitted the continuum with a linear function, ignoring absorption features, between 600 and 800 nm. The process was repeated many times, each time we randomly removed points from the datasets. The average value was adopted as the spectral slope and the standard deviation as the error. The results are shown in the first row of Table 2.

The depth of an absorption feature is computed following

$$D_\lambda[\%] = (1 - f_\lambda) \times 100,$$

where f_λ is the normalized reflectance at the wavelength λ. This formula gives the percentile value of the absorption depth of a given band and information about the quantity of the absorbing material, as well as a possible indication of the path-length traveled by the light. To compute it we first normalized the band by fitting a linear function to the band's borders and dividing the band by that function. Note that this does not change the position of the minimum, while making it easier to measure D for multiple, overlapping bands (such as the 1690 nm one). The values are reported in Table 2. All values for Eris are compatible to within the errors.

Information about the physical state of the near-surface ices was evaluated by measuring band shifts between the Eris data in several small spectral windows with respect to synthetic spectra calculated using Hapke models that describe the light reflected from particulate surfaces. We used the optical constants of pure CH_4 at 30 K (Grundy et al. 2002), the most likely temperature at Eris' surface (J. Cook, priv. comm.), to model the Eris spectrum and evaluated the goodness of the fit using a χ^2 criterion. Because the CH_4 bands at different wavelengths are caused by differing path-lengths, we used two different grain size as free parameters in the models. The grain sizes range from tens of micrometers to meters (for the weakest bands). Using such a large range of particle sizes was necessary because we only used pure CH_4; a more complete modeling (beyond the scope of this article) that includes neutral darkening and reddening material would likely result in smaller particle sizes.

The spectral model uses only the optical constants of CH_4 ice from Grundy et al. (2002) at full resolution. The optical constants were shifted from −2 to +1 nm at 0.1 nm intervals.

Table 3. Shifts of CH_4 bands with respect to the spectrum of pure CH_4 at 30 K.

Band (nm)	*a* (Å)	*b* (Å)	*c* (Å)	*d* (Å)	*e* (Å)	*f* (Å)	*g* (Å)	*h* (Å)
730	−4.1 ± 1.3	−13.9 ± 1.1	−0.3 ± 1.6	−8.0 ± 4.2	(...)	(...)	(...)	−19.7 ± 4.2
790	−0.2 ± 1.3	−6.0 ± 1.0	−4.3 ± 1.7	+0.9 ± 4.1	(...)	(...)	(...)	(...)
840	+3.9 ± 1.6	(...)	−5.9 ± 3.4	−3.3 ± 4.5	(...)	(...)	(...)	−9.5 ± 5.4
870	−3.3 ± 2.0	−5.9 ± 1.1	−8.7 ± 2.8	−3.0 ± 5.0	(...)	(...)	(...)	−21.0 ± 5.2
890	−4.2 ± 1.3	−4.7 ± 1.0	−12.4 ± 1.5	−8.1 ± 4.3	(...)	(...)	(...)	−17.6 ± 4.2
1000	−2.0 ± 1.6	(...)	(...)	(...)	(...)	(...)	(...)	(...)
1015	−2.8 ± 3.3	(...)	(...)	(...)	(...)	(...)	(...)	(...)
1135	−5.6 ± 1.6	(...)	(...)	(...)	(...)	(...)	(...)	(...)
1160	−4.5 ± 1.5	(...)	(...)	(...)	(...)	(...)	(...)	(...)
1190	−5.4 ± 2.0	(...)	(...)	(...)	(...)	(...)	(...)	(...)
1240	−1.4 ± 1.8	(...)	(...)	(...)	(...)	(...)	(...)	(...)
1335	−6.7 ± 2.1	(...)	(...)	(...)	(...)	(...)	(...)	(...)
1670	−9.4 ± 1.9	(...)	(...)	(...)	−1.7 ± 5.2	−0.3 ± 5.0	−7.7 ± 4.5	−26.3 ± 4.3
1690	−7.1 ± 3.2	(...)	(...)	(...)	−6.8 ± 5.6	−1.4 ± 5.1	−5.5 ± 5.0	+2.6 ± 5.3
1720	−10.5 ± 2.2	(...)	(...)	(...)	+3.5 ± 5.4	+3.7 ± 4.7	−8.4 ± 4.7	−24.8 ± 4.2
1800	(...)	(...)	(...)	(...)	−3.5 ± 4.3	Undet.	−10.6 ± 4.5	−23.4 ± 4.1
2200	(...)	(...)	(...)	(...)	Undet.	Undet.	−4.3 ± 6.9	−34.9 ± 4.2

Notes. Undet. = undetermined; references: (*a*) this work; (*b*) Abernathy et al. (2009); (*c*) Licandro et al. (2006); (*d*) Alvarez-Candal et al. (2008); (*e*) Guilbert et al. (2009); (*f*) Merlin et al. (2009); (*g*) Dumas et al. (2007); (*h*) Merlin et al. (2010), Pluto.

At each spectral shift, a best-fit model spectrum was derived and χ^2 was evaluated. The χ^2 measurements were then fitted to a quadratic curve to estimate the best-fit shift. To evaluate the error, we calculated a correlation matrix around the minimum and added quadratically the uncertainty of the wavelength calibration, as mentioned in corresponding works: 1 Å for this work's data and Licandro et al. (2006), 0.3 Å for Abernathy et al. (2009), and 4 Å for all the rest, as estimated by Merlin et al. (2009).

Table 3 lists the measured shifts in wavelength, and Fig. 5 illustrates the relationship between shifts and wavelength. Eris observations indicate an average blueshift of ∼5 Å, while Pluto is ∼20 Å. Note that considering all available datasets, we found no apparent relation. Nevertheless, if we consider one isolated spectrum, like XS for instance, it is possible to see that the shifts increase toward longer wavelengths (black diamonds in Fig. 5), as shown by Tegler et al. (2010) and Licandro et al. (2006, light-brown triangles) but derived from smaller datasets, while other spectra do not show any tendency unless subsets of data are used. Licandro et al.'s band at 890 nm has a blueshift comparable to that measured for Pluto. There are four Eris absorption bands that show redshifts: Alvarez-Candal et al. (2008) at 790 nm, this work's spectrum at 840 nm, and the spectra of Guilbert et al. (2009) and Merlin et al. (2009) at 1720 nm, but all of them are within three sigma from a null shift.

One feature that only appears in pure CH_4, the one at 1690 nm, shows non zero wavelength shifts. This shift might be caused by a temperature difference between the models and the actual ice on Eris' surface. But the shift is in all cases within three sigma from the laboratory position.

As mentioned above, we used only pure CH_4 at 30 K in the models. Methane ice at this temperature is in its phase I. During the modeling we determined that some bands could not be fitted with pure CH_4(I), but could be better explained by a mix of CH_4(I) and CH_4(II). This phase of methane ice, CH_4(II), occurs at temperatures below 20.4 K. The detailed results and implications are beyond the scope of the current report.

Using all the CH_4 bands in the Eris data and comparing them with similar bands in data reported for Pluto (Merlin et al. 2010), we conclude that at least some of the CH_4 on Eris appears to be diluted in another material. By analogy to Pluto we assume N_2 is the main diluting agent.

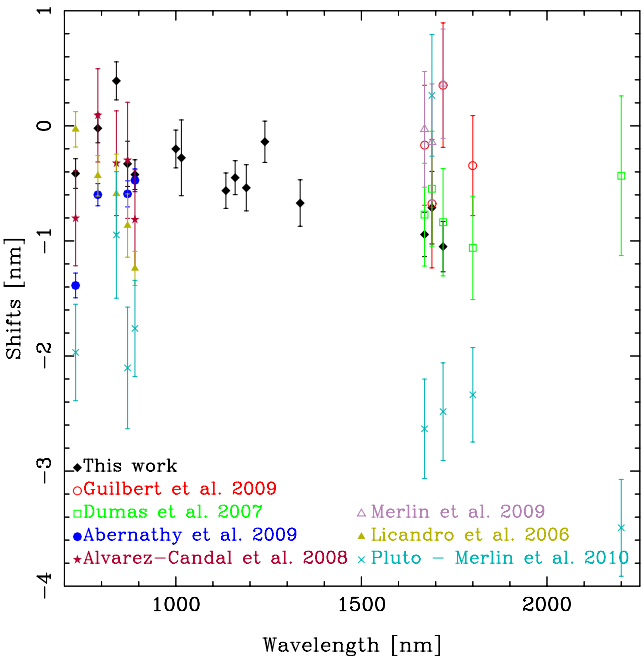

Fig. 5. Wavelength shifts for the spectra analyzed in this work.

3.2. Qualitative interpretation of the spectra

Other than the overall blue shift of the bands discussed in the previous section, there does not appear to be any systematic behavior of the individual bands analyzed, at first glance. Licandro et al. (2006) suggested that different measured shifts indicated different levels of dilution of CH_4 in an N_2 matrix: Pure CH_4 at the bottom, with the CH_4 concentration decreasing toward the surface. The proposed mechanism is based on the fact that N_2 condenses at a lower temperature than CH_4. Therefore, while approaching aphelion, CH_4 condensed first, while N_2 was still

in its gaseous phase. As Eris gets farther away from the Sun, its surface temperature decreases and N_2 starts condensing as well, thus the mixing of CH_4 in N_2 increases. This was later supported by Merlin et al. (2009), who also added a top layer of pure CH_4 as a result of the null shift they measured in near-infrared bands. In contrast, Abernathy et al. (2009) measured blueshifts for five selected absorptions and identified a correlation between the shift and the geometric albedo at the wavelength of maximum band absorption, in contrast to the behavior reported by Licandro et al. (2006). They proposed that the difference was caused by a heterogeneous surface. More recent data presented by Tegler et al. (2010) on Pluto and Eris suggest that this stratigraphic analysis of the data has overlooked that the blueshifts increase as CH_4 becomes more diluted, i.e., less abundant, in N_2.

Our results support Abernathy et al.'s (2009) suggestion: that the Eris surface is heterogeneous. Considering all data sets, there is no apparent correlation between the shift of central wavelengths of bands and the supposed depths where they form (deeper bands closer to the surface, shallower bands deeper below the surface, Fig. 6). The XS data alone show increasing blueshifts toward longer wavelengths (shallower depths), which supports the condensation mechanism proposed in Licandro et al. (2006), but using all data we cannot confirm this hypothesis. In conclusion, any stratigraphic analysis should be regarded as local, representing the part of the surface observed during the exposure.

3.3. Comparison between X-Shooter spectra

The molecule of methane ice is optically very active. It has four fundamental vibrational modes in the infrared between 3000 and 8000 nm, but all of them lead to a huge number of overtones and combinations, which can be observed with progressively diminishing absorbances into the near-infrared and visible wavelength range (Grundy et al. 2002). We can see several of these bands in our two XS spectra. Although both spectra look very similar and display the same bands, some of them display subtle differences, as can be seen in Figs. 2–4 (up to 1800 nm where the noise in the spectra does not allow detailed comparisons).

There are several factors that can be responsible for these differences. In pure methane ice, differences in the optical pathlengths followed by the scattered light result in different depths and widths for the bands. Moreover, as investigated by Grundy et al. (2002), temperature changes in the ice produce slight differences in the central peaks of these absorption bands. The situation is slightly different when CH_4 is diluted in other ices, as it could be for Eris, and the shape of the bands is influenced by the concentration of CH_4 in the matrix.

According to the classic treatment of molecules trapped in matrices, the guest CH_4 molecules can exist as isolated molecules or as clusters of various sizes in the nitrogen matrix (dimer, trimer, etc.). Quirico & Schmitt (1997a) made a detailed study for the case of methane diluted in nitrogen. In the specific case of an isolated CH_4 molecule (i.e., which has only N_2 molecules as first neighbors), the motion of the molecule is a slightly hindered rotation, thus, the CH_4 bands show a characteristic fine structure that can be seen in comparison with the shape of these bands for pure ice. However, for a cluster, the different CH_4 molecules interact with each other, the molecular rotational motion is perturbed or no longer exists, and the profile of a band can be strongly modified with respect to that of the isolated molecule (monomer). Consequently, a CH_4 absorption band can be the sum of several different bands corresponding to the monomer and other various clusters all present in the sample. Its dilution alters the shape and central frequency of the bands.

3.4. Comparison with Pluto

The immediate comparison for Eris is Pluto: both objects present CH_4-dominated spectra, and similar sizes. Pluto's surface composition is made of N_2 (the major constituent of the surface), CH_4, and CO ices. Eris' content of pure CH_4 seems to be higher than in Pluto, as witnessed by the deeper band at 1690 nm (and also the rest) and the smaller spectral shifts of the absorption bands when compared to pure CH_4. Eris' lower visible spectral slope indicates a lower content of organics than on Pluto.

The other ices, N_2 and CO, were observed and identified on Pluto by absorption bands at 2150 and 2350 nm respectively. Thus we would expect to find them on Eris. Unfortunately, owing to the low SNR in the K region of our spectra, we did not find any of them. Note that an overtone of CO is observed on Pluto at 1579 nm (Douté et al. 1999) that we do not detect. The SNR of our spectra in that region is about 15 while the spectral resolution is more than five times higher than that reported by Douté et al. (750), therefore if the CO content and the physical-chemical properties were similar on Eris, this absorption should have been detected.

Even if not directly detected, N_2 can be inferred on Eris' surface. The shifts measured above are evidence of the mixture of CH_4 with another ice. On Pluto that ice is N_2, and probably CO. The measured blueshifts for Eris are not as high as those measured in Pluto, possibly indicating a lower dilution level of CH_4 in N_2 than for Pluto.

4. Discussion

Comparing the different datasets of Eris, we do not find any evidence of major heterogeneities on its surface. For instance, the values of spectral slopes and depth of absorption bands presented in Table 2 are all compatible within the uncertainties. As a comparison, Pluto's surface has variations in albedo of up to 35% (Stern et al. 1997).

The visible slope is indicative of the presence of organics, i.e., the redder the slope, the larger the amount of organics and the lower the albedo in the visible. In the case of Eris all slopes have a value close to 3% $(100\ \mathrm{nm})^{-1}$, with error bars in the range of 1% $(100\ \mathrm{nm})^{-1}$ (see Table 2), lower than that for Pluto (12% $(100\ \mathrm{nm})^{-1}$), thus pointing to a larger fraction of organics on Pluto than on Eris. This is compatible with a higher albedo in the visible for Eris (over 0.7, e.g., Stansberry et al. 2008) compared to Pluto (averaging 0.6, Young et al. 2001).

One mechanism to form organic material is the polymerization of carbon-bearing molecules, such as CH_4. Laboratory experiments show that long-term irradiation of astrophysical ice mixtures (with the presence of simple hydrocarbons and nitrogen) results in the selective loss of hydrogen and the formation of an irradiation mantle of carbon residues (Moore et al. 1983; Johnson et al. 1984; Strazzulla et al. 1991). They also show that as the radiation dose increases, more complex polymers form, that are poor in hydrogen content, and an initially neutral-colored and high-albedo ice becomes red as the albedo in the visible decreases. More irradiation gradually reduces the albedo at all wavelengths and, finally, the material becomes very dark, neutral in color, and spectrally featureless (Andronico et al. 1987; Thompson et al. 1987). Because TNOs are exposed to ultraviolet solar radiation, the solar wind, and the flux of galactic

cosmic-rays, it is reasonable to expect that an irradiation mantle with a red color could be formed on their surfaces. A continuous deposition of fresh volatiles via sublimation and condensation acts to keep a neutral color surface with high albedo.

Assuming the lower visible spectral slope of Eris is caused purely by a lower content of organics, then the CH_4 on its surface is either younger than that of Pluto, or it is somehow protected against polymerization. One possible explanation would be the recent collapse of Eris' atmosphere, which covered its surface and masked the organics below.

Schaller & Brown (2007) showed with a simple model of loss of volatiles as a function of the surface temperature and size of the objects that Eris as well as Pluto should have retained CH_4, N_2, and CO, therefore we expect to detect them. Methane is easily seen, while N_2 can be inferred from the wavelengths shifts measured in the visible. The case of CO is more complicated, as mentioned above we do not have any detection. But, building on (i) the Schaller & Brown (2007) results; (ii) the fact that N_2 and CO are very similar molecules and therefore likely to co-exist (Scott 1976); (iii) CO observation on Pluto; CO should be present on Eris surface. We will discuss the possible cause of the non-direct detection of N_2 and CO below.

Inspecting at a more subtle level the wavelength shifts of absorption features, we find evidence of variable shifts along one single spectrum and also of the same band in different spectra, which indicate changing mixing ratios of CH_4 in another ice, probably N_2 and/or CO. Different spectra sample different regions on Eris, so, assuming that a given absorption is always produced at the same depth, most of the layers sampled by the spectra show evidence of heterogeneity (Fig. 6). Therefore, the surface of Eris is covered by a heterogeneous mix of ices: patches of pure CH_4 mixed with a dilution of CH_4 in N_2 and/or CO. In both cases, the CH_4 is so optically active that its features dominate the appearance of the spectrum.

Figure 6 was constructed by combining the information contained in Tables 2 and 3. As mentioned above, each absorption band maps a determined depth on Eris' surface, therefore, we can picture it as composed of layers. For simplicity we adopt an average value of D_λ computed from every Eris entry as a proxy of real depth: topmost layers (shorter path-lengths) have higher values of D_λ, while deeper layers (long path-lengths) have lower values of D_λ. Given all presented data, Fig. 6 shows variability between datasets, suggesting Eris' surface is heterogeneous. If we consider individual spectra or restricted datasets, relations appear. If we concentrate only on XS data, black diamonds, the topmost layers show on average the higher blueshifts and probably higher level of dilution of CH_4 in N_2 (Brunetto et al. 2008), while the deepest layer mapped by the spectra shows smaller shifts, indicating higher concentrations of CH_4.

It is important to keep in mind that the relationship between the depth of an absorption band and the path-lengths traveled by a photon is not a direct one, multiple scattering could account for long path-lengths without the need to traverse huge physical depths.

The uncertainty in the Eris rotational period unfortunately precludes any attempt of rotationally resolved spectroscopy with our current dataset. Considering the Roe et al. (2008) measurement of 1.08 ± 0.02 days for the rotation of Eris and the 48 days interval between our spectra, the indetermination on the rotational phase will add up to about one day, i.e., almost one rotational period.

Why was it not possible to directly detect either N_2 or CO in the Eris spectra? At the temperature predominating at Eris' orbit (less than 36 K), N_2 should be in its α state and therefore show

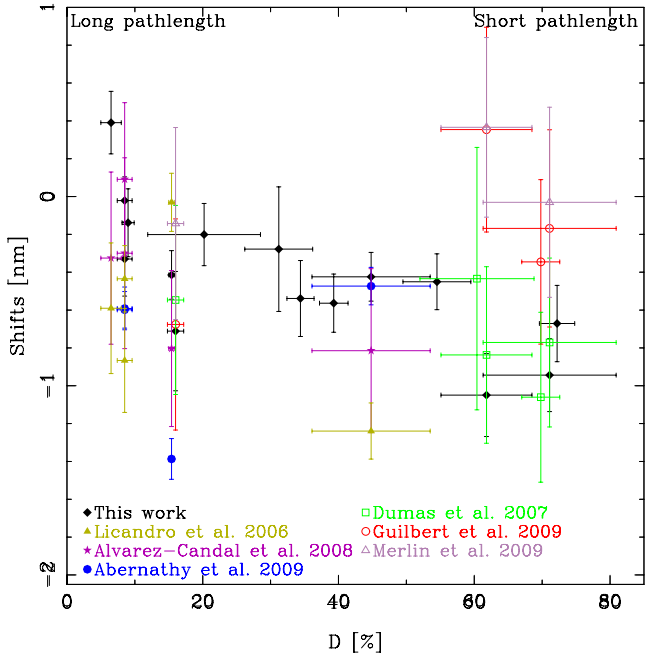

Fig. 6. Measured wavelength shifts vs. averaged D_λ. The averaged D_λ is the average value as obtained from the Eris entries in Table 2, the error bar is just the standard deviation around the average. D_λ is used as proxy of real depth in the surface, as indicated by the legends on the top of the figure. Note that with exception of the XS spectrum, filled symbols are used for absorption bands in the visible and open ones for bands in the near-infrared ($\lambda > 1000$ nm).

an absorption band at 2160 nm, the only band covered by our K-region spectra. However, this band is too narrow for the resolution of the spectra and the SNR is insufficient. Previous spectra of Eris in the near-infrared (Brown et al. 2005; Dumas et al. 2007; Guilbert et al. 2009; Merlin et al. 2009) have had better SNR than our XS spectra in the K-region, and a sufficient resolving power to detect βN_2 but have failed to detect it. One possibility is that the majority of the N_2, if present on Eris' surface, is in the α state. Quirico & Schmitt (1997b) showed that CO diluted in αN_2 has a narrow transition band. Its 0−2 transition, 2352 nm, is the strongest one and should appear in our data, unfortunately the low SNR in that region of our spectra does not allow us to impose any constraint on it. However, as mentioned in Sect. 3.3, its 0−3 transition at 1579 nm is in a region with good SNR, but we do not detect it. According to the quoted experimental setup in Quirico & Schmitt's work, this transition would need a resolving power of over 12 000 to be observable, if mixed with αN_2. This resolution is twice as high as that of XS, and therefore undetectable with our observational setup.

To detect the features at 1579 and 2352 nm of CO in a dilution with N_2 in α-state, we would need a resolving power of more than 10 000, which could be achieved with XS using its smallest slit width, 0.4″. Given a similar set up and that Eris has $m_v < 17$, we would need several hours to gather enough signal to resolve the bands. The alternative is to wait until Eris enters into a region where the surface temperature rises above that of the phase transition from αN_2 to βN_2, the features become wider and easier to resolve with less resolution, but on the other hand they also decrease in intensity. A proper rebinning of the spectrum should be enough to avoid increasing the exposure times beyond practicality. However, this will not happen until the year 2166.

5. Conclusions

Using X-Shooter, a new instrument at the ESO-Very Large Telescope, we obtained two new spectra of Eris. The spectra were obtained at high resolving power, $\lambda/\Delta\lambda \sim 5000$, covering the 300 to 2480 nm at once. We compared these datasets with those available in the literature and with a dataset of Pluto.

The main results are summarized below:

- The deeper CH_4 absorption bands on Eris indicate a higher content of CH_4 than on Pluto. This interpretation is also supported by the smaller shift of the CH_4 features from the positions of pure CH_4 when compared to Pluto.
- Neither N_2 nor CO are directly detected in our spectra, but both have been reported for Pluto.
- CH_4 is probably diluted in another ice, likely N_2 and/or CO. This can be inferred from the systematic wavelength shift of the CH_4 absorption bands in the Eris spectra from all individual observations.
- We do not see major differences between the Eris spectra, indicating that there are no large heterogeneities on the regions of its surface sampled by the two observations.
- We do observe indications of heterogeneity at a more subtle level. Central wavelengths of individual CH_4 absorption bands have different shifts when independent spectra of Eris are compared. Considering only the XS data for Eris, there is an indication of an increasing blue shift with increasing wavelength. This nicely illustrates the advantage of the XS design for simultaneously obtaining data over a broad wavelength range.

Acknowledgements. We would like to thank the X-Shooter team, who made these data available for us. N.P.A. acknowledges the support from NASA Postdoctoral Program administered by Oak Ridge Associated Universities through a contract with NASA. J.L. gratefully acknowledges support from the Spanish "Ministerio de Ciencia e Innovación" project AYA2008-06202-C03-02. J.C. acknowledges support of the NPP program. We also thank C. Dumas and F. Merlin, who kindly made their (reduced) data available to us, and an anonymous referee for the comments that helped to improve the quality of the manuscript.

References

Abernathy, M. R., Tegler, S. C., Grundy, W. M., et al. 2009, Icarus, 199, 520
Alvarez-Candal, A., Barucci, M. A., Merlin, F., Guilbert, A., & de Bergh, C. 2007, A&A, 475, 369
Alvarez-Candal, A., Fornasier, S., Barucci, M. A., de Bergh, C., & Merlin, F. 2008, A&A, 487, 741
Andronico, G., Baratta, G. A., Spinella, F., & Strazzulla, G. 1987, A&A, 184, 333
Brown, M. E., Trujillo, C. A., & Rabinowitz, D. L. 2005, ApJ, 635, L97
Brunetto, R., Caniglia, G., Baratta, G. A., & Palumbo, M. E. 2008, ApJ, 686, 1480
Carraro, G., Maris, M., Bertin, D., & Parisi, M. G. 2006, A&A, 460, L39
D'Odorico, S., Dekker, H., Mazzoleni, R., et al. 2006, SPIE, 6269, 98
Douté, S., Schmitt, B., Quirico, E., et al. 1999, Icarus, 142, 421
Duffard, R., Ortiz, J. L., Santos Sanz, P., et al. 2008, A&A, 479, 877
Dumas, C., Merlin, F., Barucci, M. A., et al. 2007, A&A, 471, 331
Giver, L. P. 1978, J. Quant. Spec. Radiat. Transf., 19, 311
Gladman, B., Marsden, B. G., & VanLaerhoven, C. 2008, Nomenclature in the outer Solar System, in The Solar System Beyond Neptune, ed. M. A. Barucci, H. Boehnhardt, D. Cruikshank, & A. Morbidelli (Tucson: Univ. of Arizona Press), 43
Guilbert, A., Alvarez-Candal, A., Merlin, F., et al. 2009, Icarus, 201, 272
Grundy, W. M., Schmitt, B., & Quirico, E. 2002, Icarus, 155, 486
Johnson, R. E., Garrett, J. W., Boring, J. W., Barton, L. A., & Brown, W. L. 1984, JGR, 89, B711
Landolt, A. U. 1992, AJ, 104, 340
Licandro, J., Grundy, W. M., Pinilla-Alonso, N., & Leisy, P. 2006, A&A, 458, L5
Merlin, F., Alvarez-Candal, A., Delsanti, A., et al. 2009, AJ, 137, 315
Merlin, F., Barucci, M. A., de Bergh, D., et al. 2010, Icarus, 210, 930
Moore, M. H., Donn, B., Khanna, R., & A'Hearn, M. F. 1983, Icarus, 54, 388
Patel, C. K. N., Nelson, E. T., & Kerl, R. J. 1980, Nature, 286, 368
Prokhvatilov, A. I., & Yantsevich, L. D. 1983, Sov. J. Low Temp. Phys., 9, 94
Quirico, E., & Schmitt, B. 1997a, Icarus, 127, 354
Quirico, E., & Schmitt, B. 1997b, Icarus, 128, 181
Ramaprasad, K. R., Caldwell, J., & McClure, D. S. 1978, Icarus, 35, 400
Roe, H. G., Pike, R. E., & Brown, M. E. 2008, Icarus, 198, 459
Schaller, E. L., & Brown, M. E. 2007, ApJ, 659, L61
Scott, T. A. 1976, Phys. Rep., 27, 89
Stansberry, J., Grundy, W., Brown, M., et al. 2008, Physical Properties of Kuiper Belt and Centaur Objects: Constraints form the Spitzer Space Telescope, in The Solar System Beyond Neptune, ed. M. A. Barucci, H. Boehnhardt, D. Cruikshank, & A. Morbidelli (Tucson: Univ. of Arizona Press), 161
Stern, S. A., Buie, M. W., & Trafton, L. M. 1997, AJ, 113, 827
Strazzulla, G., Baratta, G. A., Johnson, R. E., & Donn, B. 1991, Icarus, 91, 101
Tegler, S. C., Cornelison, D. M., Grundy, W. M., et al. 2010, ApJ, 725, 1296
Thompson, W. R., Murray, B. G. J. P. T., Khare, B. N., & Sagan, C. 1987, JGR, 92, 14933
Young, E. F., Binzel, R. P., & Crane, K. 2001, ApJ, 121, 552